AGU ADVANCING EARTH AND SPACE SCIENCE

Space Weather

RESEARCH ARTICLE
10.1029/2021SW002937

Key Points:

- Geomagnetically induced currents > 10 A occur as long-duration clusters
- Intense substorm clusters are most effective in causing such events
- Statistical relationship between the two are investigated

Correspondence to:
R. Hajra,
rajkumarhajra@yahoo.co.in

Citation:
Hajra, R. (2022). Intense, long-duration geomagnetically induced currents (GICs) caused by intense substorm clusters. *Space Weather*, *20*, e2021SW002937. https://doi.org/10.1029/2021SW002937

Received 28 SEP 2021
Accepted 27 DEC 2021

Intense, Long-Duration Geomagnetically Induced Currents (GICs) Caused by Intense Substorm Clusters

Rajkumar Hajra[1]

[1]Indian Institute of Technology Indore, Indore, India

Abstract Geomagnetically induced current (GIC) measurements at the Mäntsälä, Finland (57.9° magnetic latitude) gas pipeline from 1999 through 2019 are analyzed. It is found that the GIC events with peak intensity > 10 A are not individual peaks, but occur in clusters with duration from ∼5 to ∼38 hr when GIC values are almost continuously above ∼1.5 A. The intense, long-duration GIC > 10 A clusters (ILG_{10}) are characterized by average (median) duration of ∼17 ± 9 hr (∼14 hr), peak intensity of ∼21 ± 10 A (∼19 A), and time-integrated current flows of ∼1.0 ± 0.7 A-d (∼0.9 A-d) for all events under study. An one-to-one correlation is observed between the ILG_{10} events and intense substorm clusters characterized by average (median) duration of ∼20 ± 10 hr (∼17 hr), peak westward auroral electrojet intensity (presented by SuperMAG AL or SML index) of ∼− 2,238 ± 843 nT (∼− 2,099 nT) for all events. About 10–60 min fluctuations in the ILG_{10} events are found to be induced by substorm (SML) activity, and geomagnetic pulsations. A detailed study is presented on the local time, solar cycle, and geomagnetic dependencies of the ILG_{10} events. This will hopefully augment the predictability of the intense GICs.

Plain Language Summary Geomagnetically induced currents (GICs) are intense, low-frequency currents that flow through the gas pipelines and other long conductors. They result from the rapid changes in the geomagnetic fields induced by space weather events. In this work, a long database of GICs from a subauroral region is analyzed, and it is found that the strong GIC events with peak intensity > 10 A are long-duration events. In addition, long-duration clusters of intense substorms are responsible for such events. The results will be hopefully useful for prediction of the strong GIC events, which is important for fail-safe operation of the gas pipelines and other long ground-based conducting systems.

1. Introduction

Geomagnetically induced currents (GICs), as the name suggests, are induced by rapid changes in the geomagnetic fields, and flow in ground-based technological systems, like electric power transmission grids, oil and gas pipelines, phone cables, and railway systems (Akasofu & Aspnes, 1982; Barlow et al., 1849; Campbell, 1980; Varley, 1873). The GICs are established to be a ground manifestation of the space weather events initiating at the Sun (e.g., Kappenman, 2005; Kappernman & Albertson, 1990; Gaunt, 2016; Huttunen et al., 2008; Lakhina et al., 2021; Pirjola, 2000; Pirjola et al., 2005; Pulkkinen et al., 2008, 2009, 2017; Weigel et al., 2002; Tsurutani & Hajra, 2021, and references therein). The general scenario is as follows. The space weather events are characterized by fast, dense solar wind plasma with intense frozen-in interplanetary magnetic field (IMF). Magnetic reconnection between the IMF southward component and the northward geomagnetic field at the Earth's (dayside) magnetopause nose, subsequent downtail transport of the "open" geomagnetic field lines connected with IMF by the solar wind flow, followed by further reconnection at the far tail current sheet region are known to be the main solar wind-magnetosphere energy coupling process (Dungey, 1961). This results in disturbance of the geomagnetic fields, that induces surface geoelectric fields due to telluric currents flowing through the sub-surface structure of the Earth. The geoelectric field in turn induces GICs in gas pipelines and other long conductors.

The subauroral zone GICs have long been attributed to the auroral substorm activity (Akasofu & Aspnes, 1982; Barlow et al., 1849; Campbell, 1980). Extremely intense and damaging GICs have been reported even from high to low latitude regions during super intense geomagnetic storms (Carter et al., 2015; Clilverd et al., 2021; Kappenman, 2003; Kelly et al., 2017; Marshall et al., 2012; Torta et al., 2012; Trivedi et al., 2007; Watari et al., 2021; Zhang et al., 2015, and references therein). Recently Tsurutani and Hajra (2021) showed that the extremely intense substorms that may occur during super storms, are associated with intense ionospheric currents and rapid auroral movements (Hajra & Tsurutani, 2018; Hajra et al., 2016, 2020; Tsurutani et al., 2015). The later are

10.1029/2021SW002937

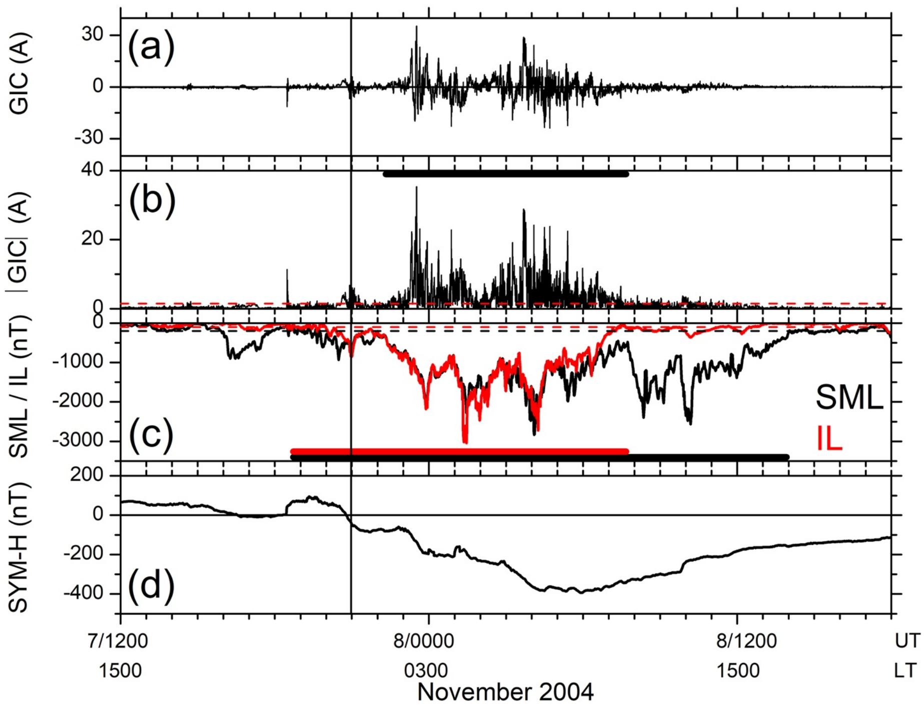

Figure 1. Intense geomagnetically induced current (GIC) events, and associated magnetic storm and auroral substorms during 7–8 November 2004. Variations of (a) GIC at Mäntsälä, (b) |GIC|, (c) auroral SML and IL indices, and (d) geomagnetic SYM-H index. The Mäntsälä local midnight is indicated by a solid vertical line. The horizontal red dashed line in panel (b) corresponds to |GIC| = 1.5 A. The horizontal dashed lines in panel (c) correspond to SML = −200 nT (black) and IL = −100 nT (red). The horizontal bar in panel (b) shows the ILG_{10} event interval. The horizontal bars in panel (c) show the intervals of the intense SML (black) and IL (red) activities (see text for details).

shown to be responsible for the strongest of the GICs in the subauroral region. In fact, using a 21-year long GIC database from Mäntsälä, Finland (57.9° magnetic latitude), it was shown that ~76% of the GIC > 30 A events were associated with extremely intense substorms when peak (minimum) westward auroral electrojet, presented by SuperMAG AL or the SML index, was less than −2,000 nT (Tsurutani & Hajra, 2021).

In this present work, the Mäntsälä GIC database, reported by Tsurutani and Hajra (2021), is re-analyzed in order to further explore the characteristics of the strong GIC > 10 A events. While Tsurutani and Hajra (2021) mainly focused on the GIC > 10 A peaks, and associated solar and geomagnetic features, the present work will investigate the temporal features, like duration, periodic variations of the intense GICs, and their associated auroral features (fluctuations, intensity, duration etc.). This study will hopefully augment our knowledge of the subauroral zone GIC activity and their predictability.

2. Database and Methods

2.1. Database

The high-resolution (10-s) GIC data analyzed in this work are taken from the Mäntsälä, Finland (geomagnetic latitude: 57.9°N, geographic latitude: 60.6°N, geographic longitude: 25.2°E) natural gas pipeline (Pulkkinen et al., 2001; Viljanen & Pirjola, 1989; Viljanen et al., 2010) for about two solar cycles, from 1 January 1999 through 31 December 2019. The GIC data are made available by the Space and Earth Observation Centre of the Finnish Meteorological Institute (https://space.fmi.fi/gic/index.php).

To study the geomagnetic conditions associated with the GIC activity, the geomagnetic SYM-H, SML and IL indices will be explored. The SYM-H index, representing the horizontal component of the symmetric ring current

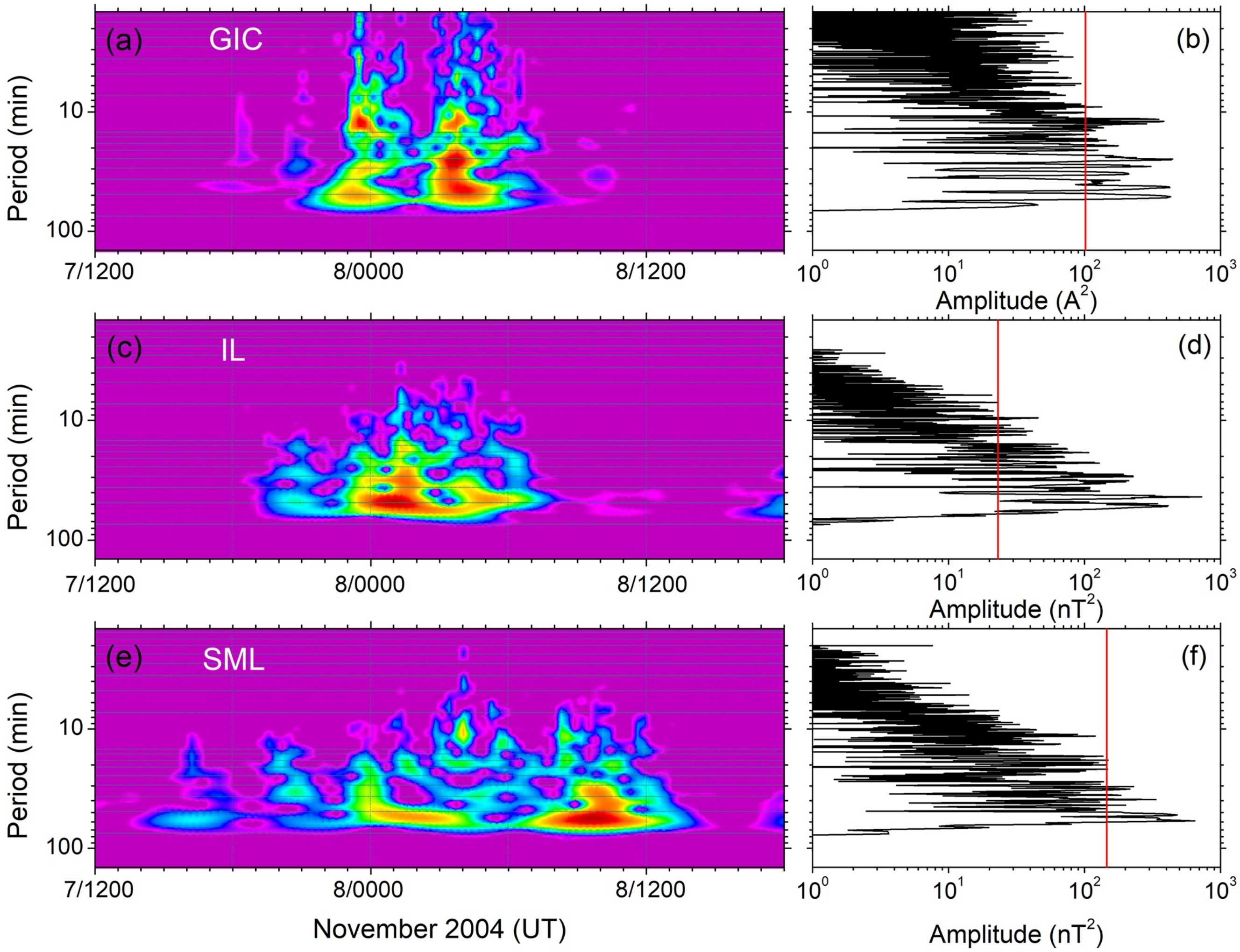

Figure 2. Wavelet and periodogram analyses of the geomagnetically induced current (GIC) (top panel), IL (middle panel), and SML (bottom panel) variations shown in Figure 1. The left panels show the *Morlet* wavelet spectra, where the red to blue colors indicate high to low amplitudes in arbitrary units. The right panels show the Lomb-Scargle periodogram analysis results, where the amplitudes of different periods are shown. The red lines in the right panels mark the 99.9% significance levels. The data period for the periodogram is the same as shown in the left panels. The periodogram analyses are performed after filtering out periodicities more than 1 hr from the time series.

(Iyemori et al., 2010; Wanliss & Showalter, 2006), exhibits decreases less than −50 nT due to the storm time ring current particle enhancement at ∼2–7 Earth radii from the Earth in its equatorial plane (Daglis et al., 1999; Frank, 1967; Hamilton et al., 1988; Shelley et al., 1972; Williams, 1987). The 1-min SYM-H indices are obtained from the World Data Center for Geomagnetism, Kyoto, Japan (http://wdc.kugi.kyoto-u.ac.jp/).

The SML index represents the westward auroral electrojet current flowing at ∼100 km altitude. This is based on all available ground-based magnetometer observations between 40°N and 80°N geomagnetic latitudes under the worldwide SuperMAG network (Gjerloev, 2009; Newell & Gjerloev, 2011), and the 1-min data are obtained from http://supermag.jhuapl.edu/. For a more direct comparison of the Mäntsälä GIC with local geomagnetic variation, the IL index will also be analyzed. It represents the westward electrojet current flowing between 47.1°N and 75.3°N geomagnetic latitudes (51.5–78.9°N geographic latitudes) and between 85.7°E and 115.1°E geomagnetic longitudes (4.8–35.1°E geographic longitudes). The 10-s IL data are collected from the International Monitor for Auroral Geomagnetic Effects (IMAGE) network (https://space.fmi.fi/image/www/il_index_panel.php; Kallio et al., 2000). It can be mentioned that Viljanen et al. (2006) reported a strong association of the the largest GICs at Mäntsälä with large geomagnetic variations at Nurmijärvi, located only at ∼30 km

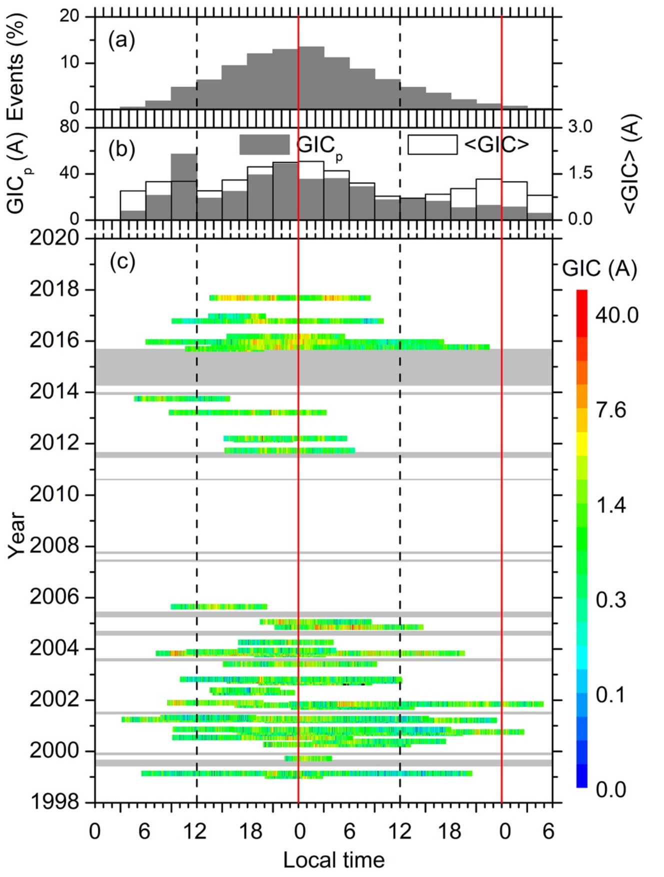

Figure 3. Local time (LT) dependence of the ILG_{10} events. (a) The percent occurrence of GIC_p >10 A at different LT sectors. (b) The LT distributions of the maximum GIC_p (gray histograms, scale on the left) and average geomagnetically induced current (GIC) strength <GIC> (empty histograms, scale on the right). (c) The GIC strengths as a function of LT (horizontal scale) and year (left hand vertical scale). Intensity corresponding to each color is given by color bar on the right. The shaded regions in the bottom panel show data gaps. The black vertical dashed lines show local noon (12 LT) and the red vertical solid lines show the local midnight (00 LT).

distance from Mäntsälä. However, as the present work is aimed to explore the GIC relationship with auroral substorm activity, the auroral indices SML and IL are more suitable for this work than any single-station magnetometer data. To study relationship between the GIC events and the ∼11-year solar cycle variation (Schwabe, 1844), yearly mean $F_{10.7}$ solar fluxes are obtained from the Laboratory for Atmospheric and Space Physics (LASP) Interactive Solar Irradiance Data Center (https://lasp.colorado.edu/lisird/data/cls_radio_flux_f107/).

2.2. Methods

From the temporal variation of the GIC absolute values (|GIC|), the intense GIC events with peaks of |GIC| > 10 A (GIC_p) were identified. Then the data were scanned both forward and backward in time to determine where |GIC| decreased below 1.5 A for 30 min or more. If the event is longer than 5 hr, it is defined as an "intense and long-duration GIC > 10 A" or ILG_{10} event. Thus, an ILG_{10} event is characterized by three criteria, namely, (a) the event has a peak |GIC| intensity greater than 10 A, (b) the event has a minimum duration of 5 hr, and (c) the GIC activity is almost continuous throughout the interval, that is, |GIC| does not drop below 1.5 A for more than 30 min at a time. It can be noted that the arbitrarily chosen 1.5 A is significantly higher than the Mäntsälä GIC measurement noise level of ∼0.1 A (Viljanen et al., 2006). The 30-min criterion is chosen based on the fact that the GIC peaks have typical duration of ∼2–15 min (Pulkkinen et al., 2003). In addition, according to Pulkkinen et al. (2001), GICs more than 10 A are quite rare at Mäntsälä, and thus can be considered as "intense". From the Mäntsälä gas pipeline GIC measurements during 1 January 1999 through 31 December 2019, 48 such ILG_{10} events are identified. For each of the ILG_{10} event, the characteristic GIC_p value, duration, the average intensity (<GIC>), and the time-integrated GIC intensity (IGIC) are estimated. The characteristic peak value (GIC_p) of an ILG_{10} event is the strongest peak or the maximum value of |GIC| during the event. IGIC is computed from area under the |GIC| curve, and expressed in the unit of A times day or A-d.

Time series plots of the SYM-H, SML and IL indices are used to identify the geomagnetic features associated with the GIC variations. SYM-H_p is computed as the peak (minimum) SYM-H intensity of the geomagnetic storm associated with each of the ILG_{10} events. The substorm clusters associated with the ILG_{10} events are characterized by the minimum SML (IL) value SML_p (IL_p), the SML (IL) duration representing the duration of the substorm cluster when SML (IL) remains less than −200 nT (−100 nT). The SML and IL thresholds are arbitrarily chosen to present significant auroral activity levels. The time-integrated value of SML (IL) during the substorm cluster, computed from area under the SML (IL) curve in the unit of nT times day or nT-d, is presented by ISML (IIL).

Statistical linear regression analysis, significance test, and statistical probability factor p (Reiff, 1990) are estimated to quantify the relationships of the GIC events with the $F_{10.7}$ solar flux, and with the geomagnetic indices. The Lomb-Scargle periodogram analysis (Lomb, 1976; Scargle, 1982) is applied to identify the significant periodicities in the GIC, IL and SML time series. The temporal variations of the periods are studied by the *Morlet* wavelet analysis (Torrence & Compo, 1998).

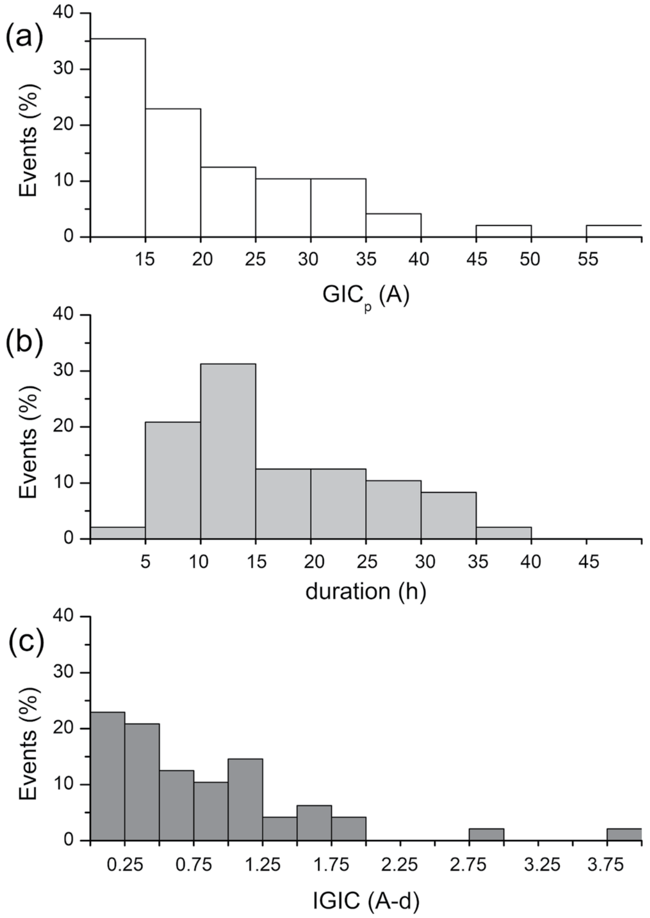

Figure 4. Statistical characteristics of the ILG_{10} events. Distributions of the events with varying (a) GIC_p, (b) duration, and (c) integrated geomagnetically induced current (GIC) intensity IGIC.

3. Results and Discussion

3.1. Intense GIC Events During 7–8 November 2004: Case Study

Figure 1a shows an example of intense GIC events at Mäntsälä occurring during 7–8 November 2004. Associated auroral substorm activity is shown by the SML and IL indices (Figure 1c), and the geomagnetic storm activity is shown by the ring current index SYM-H (Figure 1d). A detailed discussion of the solar/interplanetary features during the events, which is beyond the scope of the present work, can be found in Tsurutani and Hajra (2021).

The Mäntsälä GICs (Figure 1a) exhibit large fluctuations between the positive and negative values. From the estimated |GIC| values (Figure 1b), an intense GIC activity (ILG_{10}, shown by a black horizontal bar, Figure 1b) is noted from ∼2222 UT on 7 November (∼0122 LT on 8 November) to ∼0736 UT (∼1036 LT) on 8 November, a total duration of ∼9 hr [Mäntsälä local time (LT) = universal time (UT) + 3 hr]. During this interval, GIC was almost continuously more than 1.5 A. The GIC values seem to be low around 0200 UT on 8 November. However, a careful inspection reveals that |GIC| was below the threshold (1.5 A) only for ∼11 min. A total of 38 peaks of |GIC| > 10 A (GIC_p) are recorded during this interval. The strongest GIC peak of ∼35.36 A is recorded at ∼2331 UT on 7 November. This was local post-midnight (∼0231 LT on 8 November) at Mäntsälä. During the entire ILG_{10} interval, the time-integrated GIC (IGIC) is found to be ∼1.7 A-d.

The ILG_{10} event is found to be "embedded" inside a long-interval of intense auroral activity, as can be seen in the variations of the SML and IL indices (Figure 1c). From ∼1846 UT on 7 November to ∼1401 UT on 8 November, SML was almost continuously less than −200 nT (shown by a black horizontal bar, Figure 1c). The long-duration (∼19 hr) auroral activity or substorm cluster is characterized by a SML peak (SML_p) of −2,831 nT, and a time-integrated SML (ISML) of ∼−842 nT-d. The GIC variation is found to be more correlated with the "local" auroral activity index IL compared to the SML index. An interval of intense IL activity can be identified from ∼1846 UT on 7 November to ∼0736 UT on 8 November (shown by a red horizontal bar, Figure 1c), characterized by a peak intensity IL_p of −3,044 nT, and an integrated intensity IIL of ∼−490 nT-d.

The geomagnetic SYM-H variation shows a super intense (SYM-H < −250 nT; Gonzalez et al., 1994) geomagnetic storm during 7–8 November (Figure 1d). The storm started with a sudden impulse (SI^+) of ∼+71 nT at ∼1842 UT on 7 November, after which SYM-H decreased gradually to a peak of −394 nT at ∼0555 UT on 8 November. The strongest GICs are recorded during the main phase of the storm.

Interesting features of the ILG_{10} event shown in Figure 1 are large fluctuations in the GIC intensity, and its significant association with the fluctuating, intense and long-duration substorm cluster. The periodic variations are investigated by wavelet and periodogram analyses. Figure 2 shows the *Morlet* wavelet and Lomb-Scargle periodogram analyses of the GIC, IL and SML variations shown in Figure 1. The data period for the periodogram analyses (Figures 2b, 2d, and 2f) is the same as for the wavelet analyses (Figures 2a, 2c, and 2e). However, as we are interested in small-scale fluctuations in the parameters, the periodograms are based on the time series data after filtering out the periods more than 1 hr from the data.

Table 1
Statistical Characteristics of All 48 ILG_{10} Events

Parameters	Minimum	Maximum	Average ± SD[a]	Median
GIC_p (A)	10.1	57.1	20.8 ± 10.3	18.5
Duration (hours)	5.0	38.4	16.7 ± 8.8	14.0
IGIC (A-d)	0.2	3.9	1.0 ± 0.7	0.9

[a]SD stands for the standard deviation from the mean value.

The intense GICs are characterized by varying fluctuations of the order of a few minutes to ∼1 hr (Figure 2a). However, the period of ∼25 min has the strongest amplitude, followed by amplitudes of the periods of ∼51, ∼43, and ∼12 min (in the decreasing order of amplitude) above the 99.9% significance level (Figure 2b). While the IL *Morlet* wavelet spectrum shows a large num-

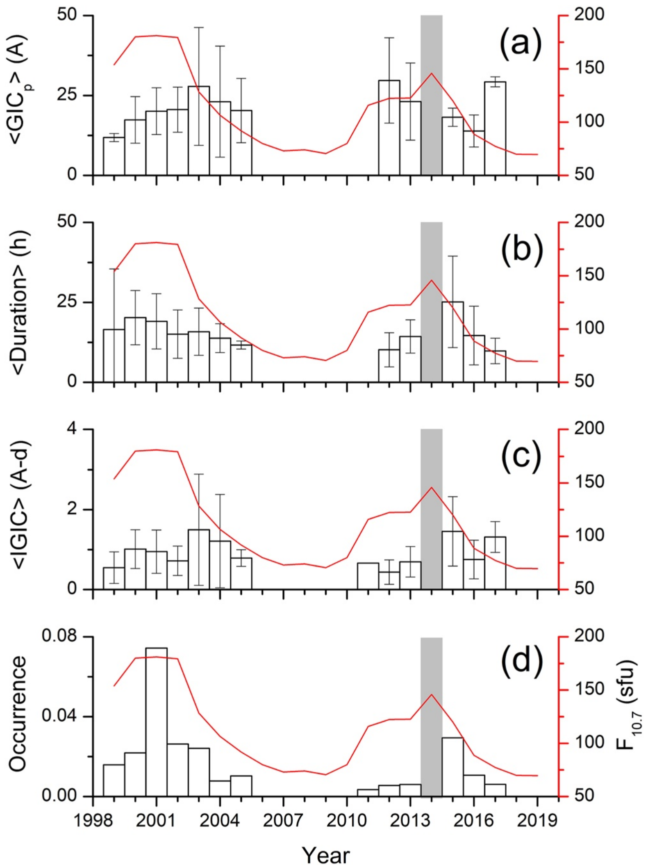

Figure 5. Solar cycle distribution of the ILG_{10} events. Histograms of the yearly averages of (a) GIC_p, (b) ILG_{10} duration, (c) IGIC, and (d) normalized occurrence rate of the ILG_{10} events. Vertical bars in panels (a–c) show the standard deviations from the corresponding yearly mean values. The gray shading in each panel indicates the geomagnetically induced current (GIC) data gaps. The continuous red curves in each panel show the yearly mean $F_{10.7}$ solar flux (scale on the right).

ber of significant fluctuations around 10 min and ∼15–60 min (Figure 2c), the strongest power is observed around 44 min (Figure 2d). The SML wavelet spectrum (Figure 2e) shows significant (above the 99.9% significance level) periodicity in the range of ∼30–60 min, with the strongest amplitude of ∼59 min, followed by ∼52, ∼39, and ∼30 min (Figure 2f). It is interesting to note that Pulkkinen and Kataoka (2006) reported similar periodicities in the Mäntsälä GICs during geomagnetic super storms. An wide-band fluctuation within the 4–150 min range was attributed to auroral substorm activity, while a narrow-band fluctuation of less than 10 min was attributed to geomagnetic Pc5 pulsations. In the present work, while GIC exhibits fluctuations in the ∼10–60 min range, IL and SML fluctuations are mainly larger than ∼15–30 min. Thus, it can be concluded that the ∼15–60 min GIC fluctuations are caused by the substorm-related (westward) auroral electrojet current variations in the same range. The smaller-scale variations in GIC might have sources in geomagnetic pulsations as suggested by Pulkkinen and Kataoka (2006).

3.2. Statistical Study

All of the 48 ILG_{10} events identified from the Mäntsälä gas pipeline GIC measurements during 1 January 1999 through 31 December 2019 are shown in the year-LT contour plot of Figure 3c. The GIC intensity is shown by the color bar at the right. The gray regions indicate data gaps, while the empty regions indicate lack of any ILG_{10} event. From the color bar, the ILG_{10} events are found to be characterized by many blue to green parts. These colors indicate the |GIC| values less than 1.5 A. This is expected as GICs exhibit small-scale variation between the positive and negative values (Figure 1a). However, these parts do not continue for more than 30 min at a time, as stated in Section 2.2. Figure 3c clearly demonstrates the solar cycle and LT dependencies of the events. Solar cycle dependence will be discussed later in more details.

Top panels (Figures 3a and 3b) show the LT dependence of the GIC peaks > 10 A, and their intensity. From the contour plot shown in Figure 3c, number of the GIC_p > 10 A at each 1-hr LT sector is counted. From this, percentage of events are computed from the total number of GIC_p > 10 A during all LT sectors. The result is shown in Figure 3a. While the long-duration events are found to extend over all LT sectors, most of the events are centered around the local midnight (Figure 3a). This local time dependence is consistent with Viljanen et al. (2006). It is due to the association of the events with the midnight substorm commencements.

In Figure 3b, GIC_p and <GIC> represent the maximum and average GIC values, respectively, at each LT sector. Interestingly, GIC_p and <GIC> exhibit two peaks-one around local midnight and another around noon (Figure 3b). Tsurutani and Hajra (2021) showed that the noontime GIC peaks are associated with the magnetospheric compressions owing to the interplanetary shock impingement.

Table 2
Results of Regression Analysis Between $F_{10.7}$ and the Geomagnetically Induced Current (GIC) Parameters

GIC parameters	Correlation coefficient *r*	*p*-value	Significance level
<GIC_p>	−0.30	0.172	< 70.0%
<Duration>	+0.51	0.045	>90.0%
<IGIC>	−0.17	0.289	<50.0%
Occurrence	+0.68	0.00068	>99.8%

Distributions of the ILG_{10} events for varying ranges of the peak GIC intensity GIC_p, duration, and time-integrated GIC intensity IGIC are shown in Figure 4. The results are summarized in Table 1. About 35% of the events are found to have GIC_p in the range 10 − 15 A, and the number of events decreases with increasing GIC_p (Figure 4a). While the event duration varies in a wide range, from ∼5 to ∼38 hr, ∼31% of the events are found to have duration between 10 and 15 hr, and ∼77% have duration

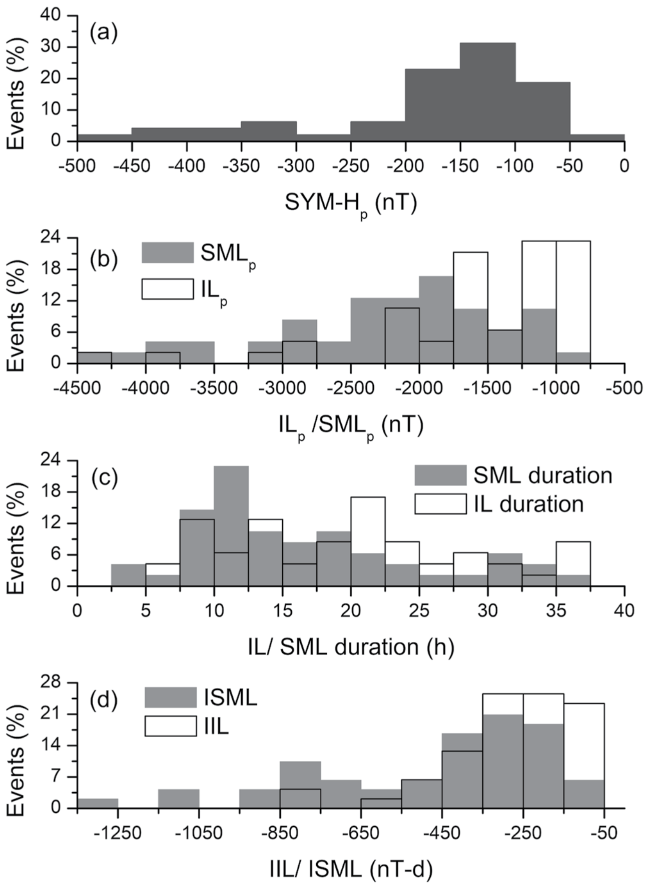

Figure 6. Geomagnetic condition associated with the ILG_{10} events. Distributions of (a) the geomagnetic storm SYM-H peak intensity SYM-H_p, (b) the substorm cluster peak intensities IL_p and SML_p, (c) the substorm cluster durations, and (d) the integrated intensities of the substorm clusters IIL and ISML associated with all ILG_{10} events.

greater than or equal to 10 hr (Figure 4b). The events have a large range of IGIC, with an average IGIC of ∼1.0 A-d for all events (Figure 4c).

Figure 5 shows the solar cycle dependence of the yearly mean GIC characteristic parameters, and the yearly normalized occurrences of the ILG_{10} events. The standard deviations from the yearly means are shown by vertical bars. The normalized occurrence rate is estimated by the total number of the ILG_{10} events in each year divided by numbers of GIC measurement days. This normalizes the effects of data gaps. From the variations of the yearly mean $F_{10.7}$ solar fluxes (red curves, scale on the right), it can be seen that the period of observation starts from the ascending phase of the solar cycle 23 and continues till the minimum following the solar cycle 24–about two solar cycles.

In solar cycle 23, the largest occurrence is recorded during the year 2001 (the year of the solar maximum), and the occurrence rate decreases with decreasing solar flux (Figure 5d). Overall occurrence rate is lower in solar cycle 24, which is the weakest solar cycle in the space age (e.g., Hajra, 2021; Hajra et al., 2021). However, the solar flux dependence of the ILG_{10} occurrences in solar cycle 24 cannot be determined as there are significant gaps of observations in the years 2014–2015 (around the solar maximum). No events are recorded around the solar minima (2006–2010, and 2018–2019) (Figure 5d). <GIC_p> seems to be enhanced during the declining phases of the solar cycles (Figure 5a). The ILG_{10} characteristic duration (Figure 5b) and <IGIC> (Figure 5c) exhibit no clear solar cycle dependence during the entire period of observation.

The relationships of the yearly normalized ILG_{10} occurrence rate, and the yearly mean characteristic parameters with the yearly mean $F_{10.7}$ solar flux are further verified by regression analysis, estimation of significance level of the regression coefficients, and the probability factor p. The p-value less than 0.05 implies that the relationship between the two parameters is statistically significant (Press et al., 1992). The results are summarized in Table 2. The maximum liner correlation coefficient r of +0.68 is recorded between the normalized ILG_{10} occurrence rate and the $F_{10.7}$ solar flux, with the significance level of more than 99.8%. The association between the two is further confirmed by $p = 0.000\ 68$. A weak correlation ($r = +0.51$, with a significance level of more than 90.0%) can also be noted between the ILG_{10} duration and the solar flux.

Figure 6 shows the geomagnetic conditions during the ILG_{10} events under study. The ILG_{10} event distributions for different ranges of SYM-H_p (Figure 6a), SML_p and IL_p (Figure 6b), SML and IL durations (Figure 6c), and ISML and IIL (Figure 6d) are shown as histograms.

The storm intensity (SYM-H_p) is found to vary in a large range, from −34 to −490 nT during all ILG_{10} events (Figure 6a). However, ∼73% of the events are associated with storms with SYM-H_p in the range of −50 to −200 nT. The associated substorm clusters are found to have SML_p between −921 and −4,418 nT, with an average (median) SML_p of ∼−2,238 ± 843 nT (∼−2,099 nT) for all events (Figure 6b). It can be noted that only ∼29% of the ILG_{10} events are associated with supersubstorm events with the SML minimum < −2500 nT (Hajra et al., 2016; Tsurutani et al., 2015), while the SML minimum ranges between −921 and −2,500 nT for 71% of the events. IL_p varies between −558 and −4,411 nT, and ∼75% of the events are associated with IL_p<−1,750 nT. The substorm cluster (SML) duration varies from ∼7 to ∼46 hr, with an average (median) duration of ∼20 ± 10 hr (∼17 hr) for all events (Figure 6c). In addition, ∼79% of the ILG_{10} events are associated with substorm clusters with duration of more than 10 hr. These results clearly demonstrate that the long-duration of the substorm cluster is more important than the intensity of an individual substorm in causing the ILG_{10} events. The combined effects of SML_p and duration are taken into account in the integrated value ISML. While ISML (IIL) exhibits a large

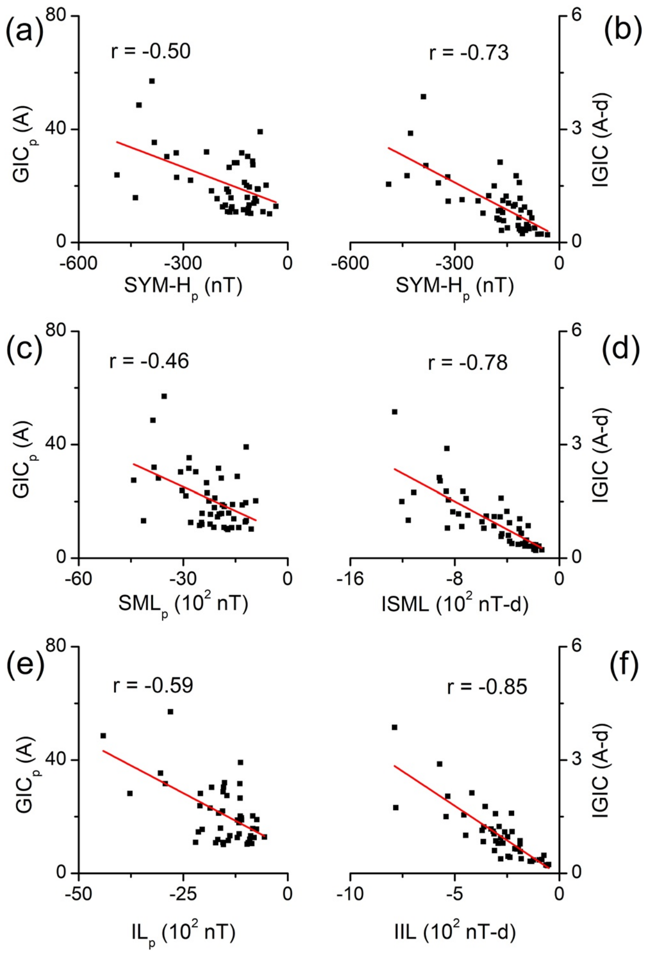

Figure 7. Variations of the ILG_{10} event peak GIC_p and integrated intensity IGIC with the the SYM-H, SML and IL peak intensities (SYM-H_p, SML_p, IL_p), and the integrated values (ISMl, IIL). Linear regression lines (red) and regression coefficients (r) are shown in each panel.

Table 3
Results of Regression Analysis Between Geomagnetically Induced Current (GIC) Parameters and Geomagnetic Parameters

Parameters	Correlation coefficient r	p-value	Significance level
GIC_p-SYM-H_p	−0.50	0.000148	>99.9%
GIC_p-SML_p	−0.46	0.000502	>99.8%
GIC_p-IL_p	−0.59	0.000013	>99.9%
IGIC-SYM-H_p	−0.73	< 0.0000001	>99.9%
IGIC-ISML	−0.78	< 0.0000001	>99.9%
IGIC-IIL	−0.85	<0.000010	>99.9%

range, ∼52% (∼87%) of the events are found to be associated with ISML (IIL) between −150 and −450 nT-d (−50 and −450nT-d).

Figure 7 shows the regression analysis between the ILG_{10} characteristic parameters and the associated geomagnetic storm intensity SYM-H_p, and the substorm cluster SML and IL features. The linear regression coefficients, corresponding significance levels, and p-values are listed in Table 3.

The ILG_{10} peak intensity GIC_p exhibits weak associations with the peak intensities SYM-H_p (Figure 7a), SML_p (Figure 7c), and IL_p (Figure 7e). However, the ILG_{10} integrated intensity IGIC exhibits significantly high associations with the magnetic storm intensity SYM-H_p (correlation coefficient $r = -0.73$) (Figure 7b), the substorm cluster integrated intensity ISML ($r = -0.78$) (Figure 7d), and IIL ($r = -0.85$) (Figure 7f). The relationships are statistically confirmed by high significance levels (>99.9%) and low p-values (Table 3). The correlation coefficients are notably higher with the local auroral activity index IL compared to more “global” indices SYM-H and SML.

4. Concluding Remarks

It is reported, for the first time, that the intense GIC > 10 A events occur as GIC clusters, continuing from ∼5 to ∼38 hr when GIC remains almost continuously more than 1.5 A. The events are thus characterized by a peak intensity, duration and an integrated value. Long-duration of the events implies that the ground-based technological systems will be impacted by such events for a significant length of time. This can be even more damaging than any impulsive, single peak GIC event. The intense and long-duration GIC events exhibit an one-to-one association with the intense substorm clusters with the peak SML intensity between ∼−1,000 and −2,500 nT, and duration of more than 10 hr. Individual substorms with higher intensity are found to be less effective in causing the GIC > 10 A events. This result clearly indicates that to effectively produce significant geomagnetic field fluctuations leading to intense GICs, both intensity of the substorms, and occurrence of multiple substorms for a sufficiently long interval of time are important.

The intense GIC clusters are characterized by ∼10–60 min periodic variations induced by the fluctuating substorm activity, and geomagnetic pulsations, as suggested by Pulkkinen and Kataoka (2006). The periodicities are significantly longer than the typical ∼2–15 min duration of the GIC peaks (Pulkkinen et al., 2003).

During the 21-year period, from 1999 through 2019, a total of 48 long-intervals of intense GICs are recorded, at a rate of ∼2 per year. However, the occurrence rate is the highest during the solar maximum, decreases with the decreasing $F_{10.7}$ solar flux, and no events were recorded during the solar minimum. This solar cycle dependence is consistent with the solar cycle dependence of the intense geomagnetic storms with the peak SYM-H intensity between −100 and −250 nT, as reported by Hajra et al. (2021), and references therein. The GIC events during the declining phases of the solar cycles seem to be enhanced in intensity on average.

Data Availability Statement

Data sources: (a) The Mäntsälä GIC data are obtained from the Space and Earth Observation Centre of the Finnish Meteorological Institute (https://space.fmi.fi/gic/index.php). (b) The SYM-H indices are obtained from the World Data Center for Geomagnetism, Kyoto, Japan (http://wdc.kugi.kyoto-u.ac.jp/). (c) The SML indices are obtained from the SuperMAG network (http://supermag.jhuapl.edu/). (d) The IL indices are obtained from the IMAGE network (https://space.fmi.fi/image/www/il_index_panel.php). (e) The $F_{10.7}$ solar fluxes are obtained from the LASP Interactive Solar Irradiance Data Center (https://lasp.colorado.edu/lisird/data/cls_radio_flux_f107/).

Acknowledgments

The work is funded by the Science and Engineering Research Board (SERB, Grant No. SB/S2/RJN-080/2018), a statutory body of the Department of Science and Technology, Government of India through the Ramanujan Fellowship. I would like to thank the reviewers for extremely valuable suggestions that substantially improved the manuscript. The author declares no real or perceived financial or any other conflicts of interests.

References

Akasofu, S.-I., & Aspnes, J. D. (1982). Auroral effects on power transmission line systems. *Nature*, *295*, 136–137. https://doi.org/10.1038/295136a0

Barlow, W. H., Barlow, P., & Culley, R. S. (1849). Vi. on the spontaneous electrical currents observed in the wires of the electric telegraph. *Philosophical Transactions of the Royal Society of London*, *139*, 61–72. https://doi.org/10.1098/rstl.1849.0006

Campbell, W. H. (1980). Observation of electric currents in the Alaska oil pipeline resulting from auroral electrojet current sources. *Geophysical Journal International*, *61*, 437–449. https://doi.org/10.1111/j.1365-246X.1980.tb04325.x

Carter, B. A., Yizengaw, E., Pradipta, R., Halford, A. J., Norman, R., & Zhang, K. (2015). Interplanetary shocks and the resulting geomagnetically induced currents at the equator. *Geophysical Research Letters*, *42*, 6554–6559. https://doi.org/10.1002/2015GL065060

Clilverd, M. A., Rodger, C. J., Freeman, M. P., Brundell, J. B., Mac Manus, D. H., Dalzell, M., et al. (2021). Geomagnetically induced currents during the 07–08 September 2017 disturbed period: A global perspective. *Journal of Space Weather and Space Climate*, *11*, 33. https://doi.org/10.1051/swsc/2021014

Daglis, I. A., Thorne, R. M., Baumjohann, W., & Orsini, S. (1999). The terrestrial ring current: Origin, formation, and decay. *Reviews of Geophysics*, *37*, 407–438. https://doi.org/10.1029/1999RG900009

Dungey, J. W. (1961). Interplanetary magnetic field and the auroral zones. *Physical Review Letters*, *6*, 47–48. https://doi.org/10.1103/PhysRevLett.6.47

Frank, L. A. (1967). On the extraterrestrial ring current during geomagnetic storms. *Journal of Geophysical Research*, *72*, 3753–3767. https://doi.org/10.1029/JZ072i015p03753

Gaunt, C. T. (2016). Why space weather is relevant to electrical power systems. *Space Weather*, *14*, 2–9. https://doi.org/10.1002/2015SW001306

Gjerloev, J. W. (2009). A global ground-based magnetometer initiative. *Eos, Transactions American Geophysical Union*, *90*, 230–231. https://doi.org/10.1029/2009EO270002

Gonzalez, W. D., Joselyn, J. A., Kamide, Y., Kroehl, H. W., Rostoker, G., Tsurutani, B. T., & Vasyliunas, V. M. (1994). What is a geomagnetic storm? *Journal of Geophysical Research*, *99*, 5771–5792. https://doi.org/10.1029/93JA02867

Hajra, R. (2021). Weakest solar cycle of the space age: A study on solar wind–magnetosphere energy coupling and geomagnetic activity. *Solar Physics*, *296*, 33. https://doi.org/10.1007/s11207-021-01774-9

Hajra, R., Marques de Souza Franco, A., Echer, E., & José Alves Bolzan, M. (2021). Long-term variations of the geomagnetic activity: A comparison between the strong and weak solar activity cycles and implications for the space climate. *Journal of Geophysical Research: Space Physics*, *126*, e2020JA028695. https://doi.org/10.1029/2020JA028695

Hajra, R., & Tsurutani, B. T. (2018). Interplanetary shocks inducing magnetospheric supersubstorms (SML < −2500 nT): Unusual auroral morphologies and energy flow. *The Astrophysical Journal*, *858*, 123. https://doi.org/10.3847/1538-4357/aabaed

Hajra, R., Tsurutani, B. T., Echer, E., Gonzalez, W. D., & Gjerloev, J. W. (2016). Supersubstorms (SML < −2500 nT): Magnetic storm and solar cycle dependences. *Journal of Geophysical Research: Space Physics*, *121*, 7805–7816. https://doi.org/10.1002/2015JA021835

Hajra, R., Tsurutani, B. T., & Lakhina, G. S. (2020). The complex space weather events of 2017 September. The *Astrophysical Journal*, *899*, 3. https://doi.org/10.3847/1538-4357/aba2c5

Hamilton, D. C., Gloeckler, G., Ipavich, F. M., Stüdemann, W., Wilken, B., & Kremser, G. (1988). Ring current development during the great geomagnetic storm of February 1986. *Journal of Geophysical Research*, *93*, 14343–14355. https://doi.org/10.1029/JA093iA12p14343

Huttunen, K. E. J., Kilpua, S. P., Pulkkinen, A., Viljanen, A., & Tanskanen, E. (2008). Solar wind drivers of large geomagnetically induced currents during the solar cycle 23. *Space Weather*, *6*, S10002. https://doi.org/10.1029/2007SW000374

Iyemori, T., Takeda, M., Nose, M., Odagi, Y., & Toh, H. (2010). *Mid-latitude geomagnetic indices ASY and SYM for 2009 (provisional)*. Internal report of data analysis center for geomagnetism and space magnetism. Japan: Kyoto University. Retrieved from http://wdc.kugi.kyoto-u.ac.jp/aeasy/asy.pdf

Kallio, E. I., Pulkkinen, T. I., Koskinen, H. E. J., Viljanen, A., Slavin, J. A., & Ogilvie, K. (2000). Loading-unloading processes in the nightside ionosphere. *Geophysical Research Letters*, *27*, 1627–1630. https://doi.org/10.1029/1999GL003694

Kappenman, J. G. (2003). Storm sudden commencement events and the associated geomagnetically induced current risks to ground-based systems at low-latitude and midlatitude locations. *Space Weather*, *1*, 1016. https://doi.org/10.1029/2003SW000009

Kappenman, J. G. (2005). An overview of the impulsive geomagnetic field disturbances and power grid impacts associated with the violent Sun-Earth connection events of 29−31 October 2003 and a comparative evaluation with other contemporary storms. *Space Weather*, *3*, S08C01. https://doi.org/10.1029/2004SW000128

Kappernman, J. G., & Albertson, V. D. (1990). Bracing for the geomagnetic storms. *IEEE Spectrum*, *27*, 27–33. https://doi.org/10.1109/6.48847

Kelly, G. S., Viljanen, A., Beggan, C. D., & Thomson, A. W. P. (2017). Understanding GIC in the UK and French high-voltage transmission systems during severe magnetic storms. *Space Weather*, *15*, 99–114. https://doi.org/10.1002/2016SW001469

Lakhina, G. S., Hajra, R., & Tsurutani, B. T. (2021). Geomagnetically induced currents. In H. K. Gupta (Ed.), *Encyclopedia of solid earth geophysics* (pp. 523–527). Cham: Pringer International Publishing. https://doi.org/10.1007/978-3-030-58631-7_245

Lomb, N. R. (1976). Least-squares frequency analysis of unequally spaced data. *Astrophysics and Space Science*, *39*, 447–462. https://doi.org/10.1007/BF00648343

Marshall, R. A., Dalzell, M., Waters, C. L., Goldthorpe, P., & Smith, E. A. (2012). Geomagnetically induced currents in the New Zealand power network. *Space Weather*, *10*, S08003. https://doi.org/10.1029/2012SW000806

Newell, P. T., & Gjerloev, J. W. (2011). Evaluation of SuperMAG auroral electrojet indices as indicators of substorms and auroral power. *Journal of Geophysical Research*, *116*, A12211. https://doi.org/10.1029/2011JA016779

Pirjola, R. (2000). Geomagnetically induced currents during magnetic storms. *IEEE Transactions on Plasma Science*, *28*, 1867–1873. https://doi.org/10.1109/27.902215

Pirjola, R., Kauristie, K., Lappalainen, H., Viljanen, A., & Pulkkinen, A. (2005). Space weather risk. *Space Weather*, *3*, S02A02. https://doi.org/10.1029/2004SW000112

Press, W. H., Teukolsky, S. A., Vetterling, W. T., & Flannery, B. P. (1992). *Numerical recipes: The art of scientific computing* (2nd ed.). Cambridge University Press.

Pulkkinen, A., Bernabeu, E., Thomson, A., Viljanen, A., Pirjola, R., Boteler, D., et al. (2017). Geomagnetically induced currents: Science, engineering, and applications readiness. *Space Weather*, *15*, 828–856. https://doi.org/10.1002/2016SW001501

Pulkkinen, A., & Kataoka, R. (2006). S-transform view of geomagnetically induced currents during geomagnetic superstorms. *Geophysical Research Letters*, *33*, L12108. https://doi.org/10.1029/2006GL025822

Pulkkinen, A., Pirjola, R., & Viljanen, A. (2008). Statistics of extreme geomagnetically induced current events. *Space Weather*, *6*, S07001. https://doi.org/10.1029/2008SW000388

Pulkkinen, A., Taktakishvili, A., Odstrcil, D., & Jacobs, W. (2009). Novel approach to geomagnetically induced current forecasts based on remote solar observations. *Space Weather*, *7*, S08005. https://doi.org/10.1029/2008SW000447

Pulkkinen, A., Thomson, A., Clarke, E., & McKay, A. (2003). April 2000 geomagnetic storm: Ionospheric drivers of large geomagnetically induced currents. *Annales Geophysicae*, *21*, 709–717. https://doi.org/10.5194/angeo-21-709-2003

Pulkkinen, A., Viljanen, A., Pajunpää, K., & Pirjola, R. (2001). Recordings and occurrence of geomagnetically induced currents in the Finnish natural gas pipeline network. *Journal of Applied Geophysics*, *48*, 219–231. https://doi.org/10.1016/S0926-9851(01)00108-2

Reiff, P. H. (1990). The use and misuse of statistics in space physics. *Journal of Geomagnetism and Geoelectricity*, *42*, 1145–1174. https://doi.org/10.5636/jgg.42.1145

Scargle, J. D. (1982). Studies in astronomical time series analysis. II. statistical aspects of spectral analysis of unevenly spaced data. *The Astrophysical Journal*, *263*, 835–853. https://doi.org/10.1086/160554

Schwabe, H., & Schwabe, H. (1844). Sonnen–Beobachtungen im Jahre 1843. *Astronomische Nachrichten*, *21*, 233–235. https://doi.org/10.1002/asna.18440211505

Shelley, E. G., Johnson, R. G., & Sharp, R. D. (1972). Satellite observations of energetic heavy ions during a geomagnetic storm. *Journal of Geophysical Research*, *77*, 6104–6110. https://doi.org/10.1029/JA077i031p06104

Torrence, C., & Compo, G. P. (1998). A practical guide to wavelet analysis. *Bulletin of the American Meteorological Society*, *79*, 61–78. https://doi.org/10.1175/1520-0477(1998)079<0061:apgtwa>2.0.co;2

Torta, J. M., Serrano, L., Regué, J. R., Sánchez, A. M., & Roldán, E. (2012). Geomagnetically induced currents in a power grid of northeastern Spain. *Space Weather*, *10*, S06002. https://doi.org/10.1029/2012SW000793

Trivedi, N. B., Vitorello, I., Kabata, W., Dutra, S. L. G., Padilha, A. L., Bologna, M. S., et al. (2007). Geomagnetically induced currents in an electric power transmission system at low latitudes in Brazil: A case study. *Space Weather*, *5*, S04004. https://doi.org/10.1029/2006SW000282

Tsurutani, B. T., & Hajra, R. (2021). The interplanetary and magnetospheric causes of geomagnetically induced currents (GICs) > 10 A in the Mäntsälä Finland pipeline: 1999 through 2019. *Journal of Space Weather and Space Climate*, *11*, 23. https://doi.org/10.1051/swsc/2021001

Tsurutani, B. T., Hajra, R., Echer, E., & Gjerloev, J. W. (2015). Extremely intense (SML ≤ -2500 nT) substorms: Isolated events that are externally triggered? *Annales Geophysicae*, *33*, 519–524. https://doi.org/10.5194/angeo-33-519-2015

Varley, C. (1873). Discussion of a few papers on earth currents. *Journal of the Society of Telegraph Engineers*, *2*, 111–123. https://doi.org/10.1049/jste-1.1873.0033

Viljanen, A., Koistinen, A., Pajunpää, K., Pirjola, R., Posio, P., & Pulkkinen, A. (2010). Recordings of geomagnetically induced currents in the Finnish natural gas pipeline-Summary of an 11-year period. *Geophysica*, *46*, 59–67.

Viljanen, A., & Pirjola, R. (1989). Statistics on geomagnetically-induced currents in the Finnish 400 kV power system based on recordings of geomagnetic variations. *Journal of Geomagnetism and Geoelectricity*, *41*, 411–420. https://doi.org/10.5636/jgg.41.411

Viljanen, A., Pulkkinen, A., Pirjola, R., Pajunpää, K., Posio, P., & Koistinen, A. (2006). Recordings of geomagnetically induced currents and a nowcasting service of the Finnish natural gas pipeline system. *Space Weather*, *4*, S10004. https://doi.org/10.1029/2006SW000234

Wanliss, J. A., & Showalter, K. M. (2006). High-resolution global storm index: *Dst* versus SYM-H. *Journal of Geophysical Research*, *111*, A02202. https://doi.org/10.1029/2005JA011034

Watari, S., Nakamura, S., & Ebihara, Y. (2021). Measurement of geomagnetically induced current (GIC) around Tokyo, Japan. *Earth, Planets and Space*, *73*, 102. https://doi.org/10.1186/s40623-021-01422-3

Weigel, R. S., Vassiliadis, D., & Klimas, A. J. (2002). Coupling of the solar wind to temporal fluctuations in ground magnetic fields. *Geophysical Research Letters*, *29*, 21-1–21-4. https://doi.org/10.1029/2002GL014740

Williams, D. J. (1987). Ring current and radiation belts. *Reviews of Geophysics*, *25*, 570–578. https://doi.org/10.1029/RG025i003p00570

Zhang, J. J., Wang, C., Sun, T. R., Liu, C. M., & Wang, K. R. (2015). GIC due to storm sudden commencement in low-latitude high-voltage power network in China: Observation and simulation. *Space Weather*, *13*, 643–655. https://doi.org/10.1002/2015SW001263